sp³−sp² vs sp³−sp³ C−C Site Selectivity in Rh-Catalyzed Ring Opening of Benzocyclobutenol: A DFT Study

Lina Ding,[†] Naoki Ishida,[‡] Masahiro Murakami,[‡] and Keiji Morokuma*,[†]

[†]Fukui Institute for Fundamental Chemistry, Kyoto University, Kyoto 606-8103, Japan
[‡]Department of Synthetic Chemistry and Biological Chemistry, Kyoto University, Katsura, Kyoto 615-8510, Japan

Ⓢ *Supporting Information*

ABSTRACT: The $C_{sp^3}-C_{sp^2}$ vs $C_{sp^3}-C_{sp^3}$ site selectivity in the C−C bond activation in Rh-catalyzed ring opening of benzocyclobutenol was systematically investigated using density functional theory (DFT). The catalytic cycle includes three elementary steps: the proton transfer from the substrate to a rhodium hydroxide, the C−C cleavage, and the proton transfer from water onto a carbon forming the final product with regeneration of the rhodium hydroxide. The site selectivity is determined by the C−C cleavage step; the $C_{sp^3}-C_{sp^2}$ cleavage is favored over the $C_{sp^3}-C_{sp^3}$ cleavage because the former transition state is stabilized by an interaction between the benzene ring of the substrate and Rh. DMSO, a more polar solvent, reduces the site selectivity as the more polar $C_{sp^3}-C_{sp^3}$ transition state (TS) is stabilized more than the $C_{sp^3}-C_{sp^2}$ TS and decreases the advantage of the latter TS. DPPF ligand is bulky, and the steric repulsion on the tighter $C_{sp^3}-C_{sp^2}$ TS causes the loss of the site selectivity. For the even more crowded $Rh(P(t\text{-}Bu)_3)_2$ catalyst, one phosphine has to dissociate before the C−C cleavage reaction takes place, and the advantage of the $C_{sp^3}-C_{sp^2}$ TS is regained for the less crowded $RhP(t\text{-}Bu)_3$ active catalyst.
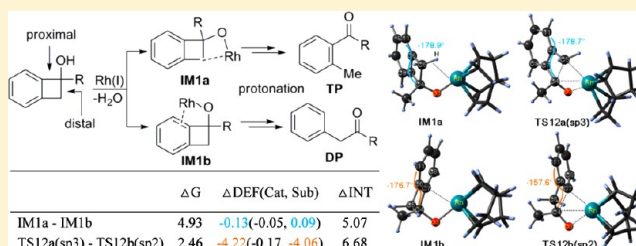
1. INTRODUCTION

Transition-metal catalysis has made significant and continual contributions to the development of synthetic organic chemistry, which has opened the wide synthetic applications of nonpolar and highly inert σ-bonds such as C−H bonds.[1] The recent evolution has rendered it possible to cleave C−C single bonds in a catalytic manner and utilize them in organic synthesis. However, the available means to cleave C−C bonds are still in its infancy[2] and generally rely on substrate-specific strategies such as ring strain, aromatization, chelating, or coordinating assistance to induce C−C bond cleavage.[2]

Transition-metal catalysts induce ring opening of cyclobutanols.[3] The ring-opening process has been extended to various reactions to restructure carbon frameworks.[4] Very recently, ring opening of benzocyclobutenols[5] with site-selective cleavage of the $C_{sp^3}-C_{sp^2}$ ("proximal") bond (Scheme 1) to produce DP was reported. The site-selective ring opening at the $C_{sp^3}-C_{sp^2}$ bond is complementary to the ring opening at $C_{sp^3}-C_{sp^3}$ ("distal") bond induced by heating, photo irradiation, and treatment with a base to produce TP via reactive o-quinodimethanes. Experimentally, the site selectivity is significantly influenced by the ligands on the Rh(I) and the solvent. For instance, as shown in Table 1 and Scheme 2, the use of cycloocta-1,5-diene (cod) as the ligand in toluene shows a strong preference for the $C_{sp^3}-C_{sp^2}$ bond cleavage, while 1,1′-bis(diphenylphosphino)ferrocene (DPPF) and $P(t\text{-}Bu)_3$ show reversed or low site selectivity. The polar DMSO solvent reduces the site selectivity. A proposed mechanism for the ring

Scheme 1. Dichotomy in Ring Opening of Benzocyclobutenols[a]
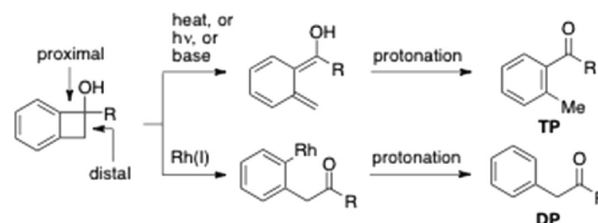
[a]Adapted from ref 5a.

## Table 1. Experimentally Observed Site Selectivities

conditions	DP	TP
[Rh(OH)(cod)]₂ in toluene	89%	0%
[Rh(OH)(cod)]₂ in DMSO	63%	31%
[Rh(OH)(DPPF)]₂ in toluene	35%	50%
Rh(acac)(CH₂CH₂)₂/P(t-Bu)₃ (1/2) in toluene[a]	74%	14%

[a]Adapted from ref 5a, DP is the product of the $C_{sp^3}-C_{sp^2}$ ("proximal") bond ring opening and TP is the product of the $C_{sp^3}-C_{sp^3}$ ("distal") bond ring opening. acac: acetylacetonate

opening of benzocyclobutenols is via proton transfer followed by β-carbon elimination.[5]

Scheme 2. Catalysts with Different Ligands, cod, DPPF, and P(t-Bu)$_3$

[Rh(OH)(cod)]$_2$

DPPF

P(t-Bu)$_3$
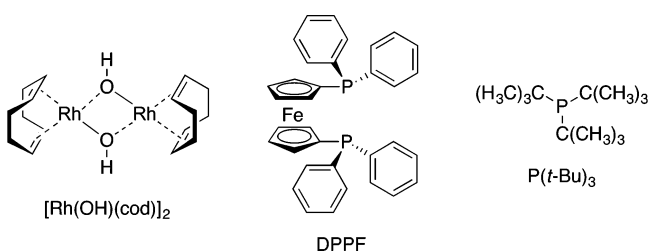
Further investigations on the mechanism are highly desired to understand these reactions in detail. Clarification of the factors that influence carbon−carbon bond cleavage could be helpful for deeper understanding of the general area of carbon−carbon activation and may lead to new methodology for restructuring carbon frameworks. Theoretical studies would be very profitable toward this goal. A mechanistic picture including the potential energy surfaces, energetic and the nature of equilibrium structures is very important to describe the nature of reaction pathways. However, computational investigations on the carbon−carbon bond activation by transition metals are limited to the C−CN bond and some special substrates.[6]

In the present work, we systematically investigated the mechanism of the Rh-catalyzed ring opening of benzocyclobutenol by a density functional theory (DFT). The catalytic cycle has been found to include three steps: deprotonation of benzocyclobutenol to form Rh(I) alkoxide, C−C bond cleavage (β-carbon elimination), and proton transfer from water onto a carbon to form the product with regeneration of the active rhodium hydroxide. The present results successfully depict the cause of the site selectivity and explain well its ligands dependency and solvent influence, which should be useful for designing new catalysts and improving site selectivity. The mechanistic picture described by the present computational study provides deeper insight into understanding of C−C bond cleavage.

2. COMPUTATIONAL MODEL AND DETAILS

To fully understand the reaction mechanism of the Rh-catalyzed ring opening of benzocyclobutenols, we employed a DFT[7] to investigate the electronic structure and energetics along the reaction potential energy surface (PES), where the effect of solvents (from less polar toluene to polar DMSO) on the site selectivity was considered with geometry optimization with the polarizable continuum medium (PCM) model.[8] Here, Rh-catalyst with cod was chosen as the representative model because of its best site selectivity among ligands (L) examined in the experiments (Scheme 2, Table 1). All calculations were performed with Gaussian 09[9] software package.

When studying the model catalyst [Rh(OH)(cod)]$_2$ in the solvent toluene, the DFT method with the Becke's three-parameter hybrid functional,[10] LYP correlation functional[11] (B3LYP) functional together with PCM model (radii = UFF, ε = 2.3741 for toluene) was utilized to fully optimize all the stationary points on the PES without symmetry or geometric constraints, in conjunction with effective core potentials (ECPs) with the SDD basis sets for rhodium and the 6-31G*[12] basis sets for other elements (called BS1). It should be noted that different density functionals may vary from each other in predicting reaction barriers. Our evaluation of two typical density functionals (M06,[13] B3LYP) in gas phase showed that they predicted similar results and led to the same discussion and conclusions for the studied rhodium systems (see Figure S1a,b, hereafter referred to with label S). Herein we chose the widely used B3LYP method for our study. Frequency calculations at the B3LYP/BS1 level of theory were

carried out to confirm the nature of the stationary points. The zero-point energies and the thermal corrections at 298.15 K and 1 atm were obtained with the harmonic approximation at the optimized structures. Intrinsic reaction coordinates (IRCs)[14] were calculated to verify the connectivity of the transition states to relevant reactants and products. Then, the larger basis set 6-311G** for other elements (termed as BS2) was employed to further refine the relative energies by single-point calculations.

To consider the effects of solvent environment on the site selectivity, we reoptimized the intermediate and transition-state structures involved in the key C−C bond cleavage step within polar DMSO (PCM, radii = UFF, ε = 46.826) at the B3LYP/BS1 level and refined the relative energies by single point calculations at B3LYP/BS2 level.

To explain the experimental observation that different ligands lead to different results, two other active species where the cod ligand was replaced by DPPF and two P(t-Bu)$_3$ ligands (Scheme 2) were employed in the study of the key C−C bond cleavage step. The electronic structure and energetics along the PES of the C−C bond cleavage are investigated at B3LYP/BS1 level, where both Rh and Fe were treated with SDD basis sets and ECPs and other elements (C, H, O, P) with the 6-31G* basis set.

To gain insight into the site selectivity in detail, the energy decomposition analysis (EDA) at B3LYP/BS2 level was carried out for two intermediates and two transition-state structures involved in the C−C bond cleavage step. Based on test calculations, each B3LYP/BS1 optimized structure was divided into a pair of ions (A and B), where the representative labels A and B are the catalyst and substrate parts, respectively. As is shown in Scheme 3, the deformation (DEF) energy

Scheme 3. EDA between Two Optimized Structures

$$\Delta DEF = DEF_2 - DEF_1$$
$$\Delta INT = INT_2 - INT_1$$
$$\Delta E = \Delta DEF - \Delta INT$$
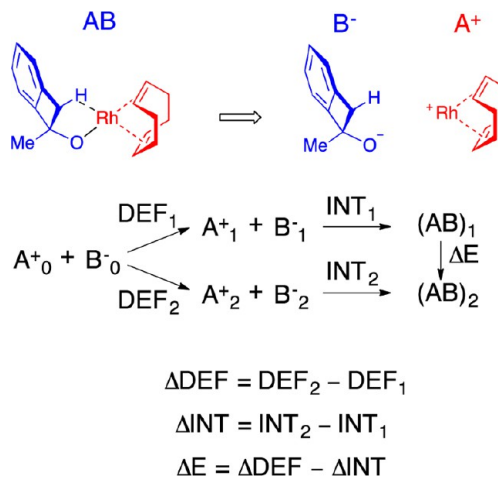
of a structure (say 1) is defined to be the sum of energies of isolated A and B (denoted as A_1 and B_1) in the optimized structure of 1, relative to the reference energy, sum of energies of the optimized structures, A_0 and B_0. The interaction energy (INT) is defined to be the energy of the optimized structure of 1 ((AB)$_1$) relative to the pair of ions (A_1 and B_1). Using these energy terms, the energy difference ΔE between two optimized structures, (AB)$_1$ and (AB)$_2$, can be divided into two terms, the deformation (ΔDEF) difference and interaction energy difference (ΔINT).

In order to take into account the dispersion contributions, we also performed calculations at B3LYP-D3/BS2//B3LYP/BS1 and B3LYP-D3/BS2//B3LYP-D3/BS2 levels for some important steps, as shown in Figure S4a,b and Tables S4−S7. The results indicate that dispersion correction does not change the overall picture of the reaction mechanism and stereoselectivity, except for one case of DPPF as will be discussed in Section 3.5, and the energetics at theB3LYP/BS2// B3LYP/BS1 level without dispersion will be used in the main text for discussion.
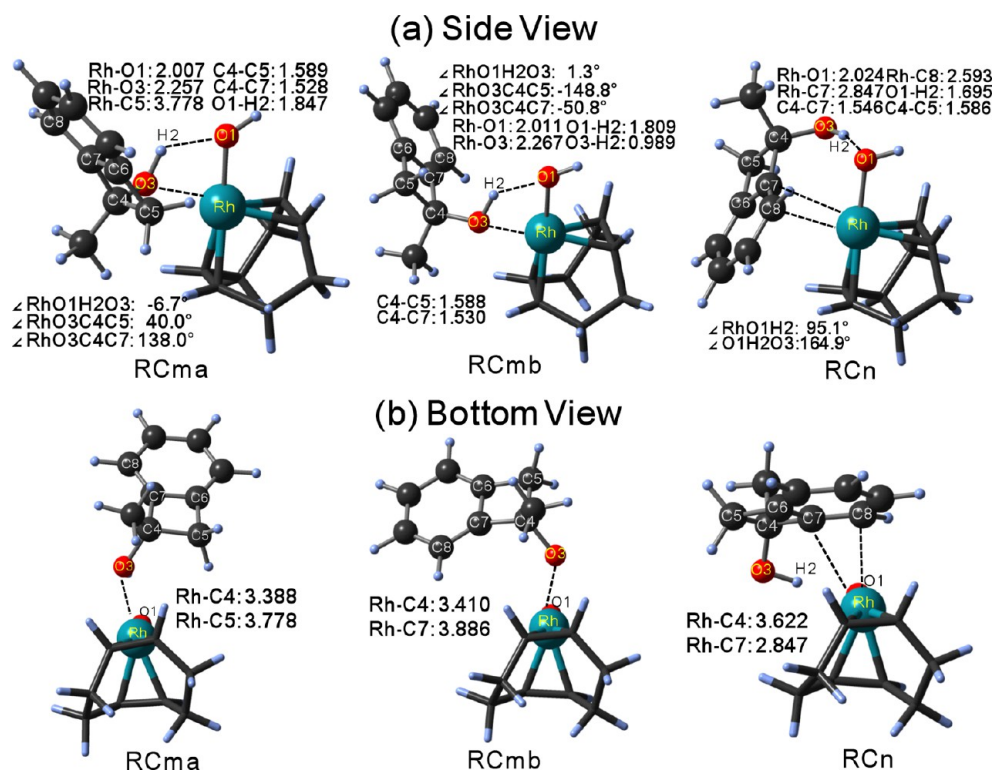
(a) Side View

∠RhO1H2O3: -6.7°
∠RhO3C4C5: 40.0°
∠RhO3C4C7: 138.0°

Rh-O1: 2.007 C4-C5: 1.589
Rh-O3: 2.257 C4-C7: 1.528
Rh-C5: 3.778 O1-H2: 1.847

RCma

∠RhO1H2O3: 1.3°
∠RhO3C4C5: -148.8°
∠RhO3C4C7: -50.8°
Rh-O1: 2.011 O1-H2: 1.809
Rh-O3: 2.267 O3-H2: 0.989

C4-C5: 1.588
C4-C7: 1.530

RCmb

Rh-O1: 2.024 Rh-C8: 2.593
Rh-C7: 2.847 O1-H2: 1.695
C4-C7: 1.546 C4-C5: 1.586

∠RhO1H2: 95.1°
∠O1H2O3: 164.9°

RCn

(b) Bottom View

Rh-C4: 3.388
Rh-C5: 3.778

RCma

Rh-C4: 3.410
Rh-C7: 3.886

RCmb

Rh-C4: 3.622
Rh-C7: 2.847

RCn

Figure 1. Atomic labels and selected geometrical parameters (in Å and °) in the reactant complexes **RCma**, **RCmb**, and **RCn**.

Scheme 4. Reaction Pathways of Rh-Catalyzed Ring Opening of Benzocyclobutenol
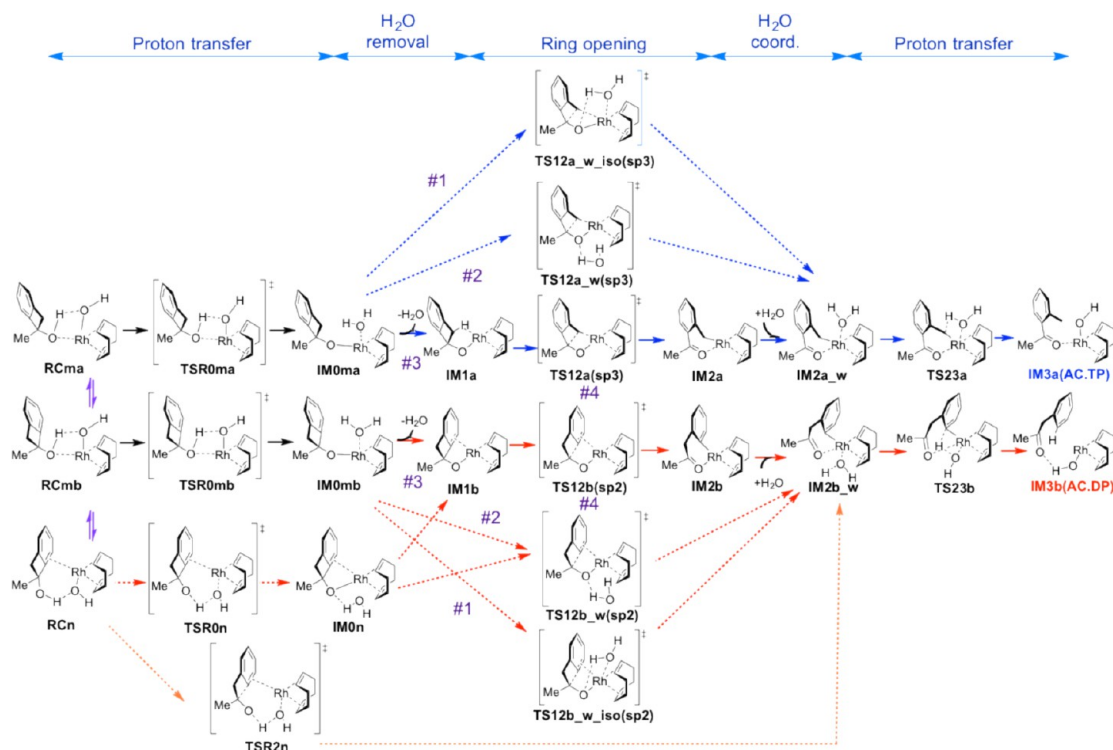
We use the Gibbs free energy throughout the paper. Both enthalpy and free energy lead to same discussion and conclusions for this system, except for the steps where one water molecule is dissociated (see Table S1). We calculated the Gibbs free energy in full consideration of translational and rotational contributions as well as vibrational contribution. This may give an overestimation of the entropy effect for the system where the dissociated water molecule is in solution and the entropy may be partially quenched.[15]

3. RESULTS AND DISCUSSION

3.1. Plausible Active Species and Reactant Complexes. The $[\text{Rh(OH)(cod)}]_2$ system, which experimentally
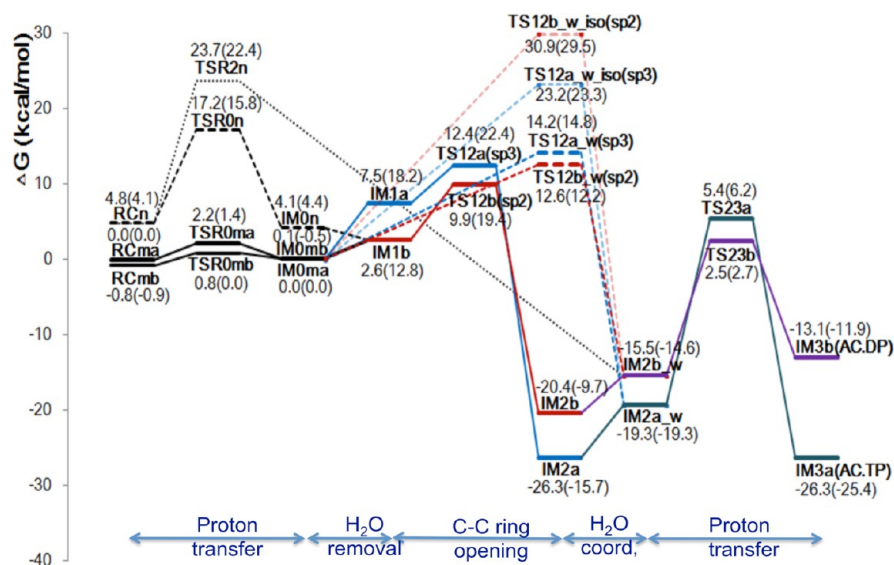
Figure 2. Gibbs free energy profiles (and enthalpies in parentheses) for the site-selective reaction of Rh-catalyzed ring opening of benzocyclobutenol, at B3LYP/BS2//B3LYP/BS1 level in toluene, relative to **RCma**.
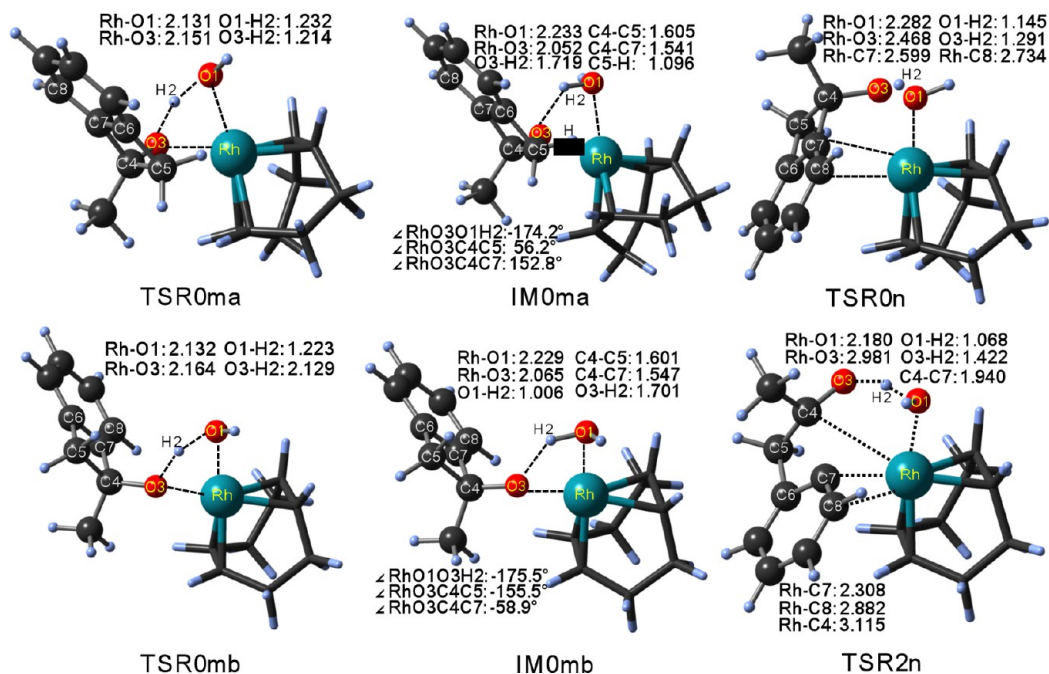

Figure 3. Selected geometrical parameters (in Å) of proton-transfer transition states **TSR0ma, TSR0mb, TSR0n**, and **TSR2n** and products **IM0ma** and **IM0mb**.

produced the best site selectivity,[5] was chosen to study the working mechanism. Based on the kinetic study[16] of a related $[Rh(OH)(cod)]_2$-catalyzed reaction, the plausible active catalyst (**AC**) has been assumed to be the monomer, since the dimer is a resting state of catalysis and nonreactive. The coordinatively unsaturated rhodium center in the monomer would facilely accept Lewis basic ligands to form tetra-coordinated species. In addition, hydrogen bonding between the hydroxide ligand on rhodium and the proton of benzocyclobutenol would further stabilize the complexes and facilitate the proton transfer. Therefore, three catalyst-substrate complexes (**RCma, RCmb**, and **RCn**) shown in Figure 1, can be taken as the starting points leading to the initial proton transfer, which turned out to be essential for lowering the

barrier of the C−C bond cleavage. **RCma** and **RCmb** bear a coordination bond between the benzocyclobutenol oxygen and the rhodium and a H-bonding between the alcoholic hydrogen and the hydroxide oxygen to form a four-membered ring. The two isomers are interconvertible through rotation along the O3−C4 single bond. **RCn** has an η^2-coordination bond between the benzene ring and the rhodium in place of a coordination bond between the benzocyclobutenol oxygen and the rhodium, in addition to a H-bonding between the alcoholic hydrogen and the hydroxide oxygen.

Although we also found pathways *without* proton transfer for the Rh-catalyzed C−C bond cleavage, as shown in Figure S2 and Table S2, they are substantially higher in energy than the present pathways that accompany the proton transfer and will

not be discussed further. We also calculated thermal C−C bond cleavage pathways without catalyst (as shown in Scheme S1 and Figure S3). In agreement with experiments, these pathways have high activation barriers (>30 kcal/mol) and the C_{sp^3}−C_{sp^3} activation is much more preferred over the C_{sp^3}−C_{sp^2} activation.

In the optimized geometries of **RCma**, **RCmb**, and **RCn** (Figure 1), the H-bonding distance between the hydroxide oxygen and the alcoholic hydrogen (O1···H2) is 1.847 Å in **RCma**, 1.809 Å in **RCmb**, and 1.695 Å in **RCn**. Relative to the bonds C4−C5/C4−C7 (1.595/1.527 Å) in the free benzocyclobutenol, there is no significant change in the corresponding bonds in **RCma** (1.589/1.528 Å), **RCmb** (1.588/1.530 Å), and in **RCn** (1.586/1.546 Å), which indicates that no substantial activation of C_{sp^3}−C_{sp^3} or C_{sp^3}−C_{sp^2} has taken place during the coordination with the catalyst. The distances from Rh to C4/C5 in **RCma** or to C4/C7 in **RCmb** and **RCn** are 3.388/3.778, 3.410/3.886, and 3.622/2.847 Å, respectively, showing that the cleaving C−C bonds are still too far away from Rh in these reactant complexes and that the initial proton-transfer process is necessary for C−C bond cleavage. Energetically, **RCma** and **RCmb** are more stable than **RCn** by 4.8 and 5.6 kcal/mol, respectively.

The reaction pathways found for the present catalytic system starting from **RCma**, **RCmb** and **RCn** are shown in Scheme 4. The energetics along the reaction pathways is shown in Figure 2. In the following sections, we will present in-depth discussions on the details of the reaction pathways.

3.2. Initial Proton-Transfer Mechanism. Starting from the more stable reactant complexes, **RCma** and **RCmb**, two transition-state structures (referred as **TSR0ma** and **TSR0mb**) were obtained (Figure 3) for the initial proton transfer from the cyclobutanol substrate to the hydroxy ligand on Rh (Scheme 4). The **TSR0ma** connects **RCma** to the intermediate **IM0ma** with a small free-energy barrier of 2.2 kcal/mol, while the **TSR0mb** connects **RCmb** to **IM0mb** with even less barrier of 1.6 kcal/mol (Figure 2). Therefore both pathways are likely to participate, giving two intermediates (**IM0ma** and **IM0mb**, Figure 3) that are also close in energy. Although not examined carefully, two isomeric structures **RCma** and **RCmb** as well as **IM0ma** and **IM0mb** are likely to isomerize to each other easily by rotation along Rh−O3 single bond.

On the other hand, two transition-state structures were found starting from less stable **RCn** (Figure 3). One is **TSR0n** that leads to a proton-transfer intermediate **IM0n** with a barrier of 17.2 kcal/mol, which is much higher than the pathways starting from **RCma** or **RCmb** and can be neglected. The other is **TSR2n**, with a barrier of 23.7 kcal/mol, that involves the proton transfer with a concerted cleavage of the C7−C4 bond (a C_{sp^3}−C_{sp^2} bond). Optimization of this TS using the M06 method converged to **TSR0n** for the stepwise pathway. Thus the concerted pathway does not exist or has high energy, if exists, and can also be ignored.

The most likely pathways for the first step are the stepwise pathways via **RCma** → **TSR0ma** → **IM0ma** and **RCmb** → **TSR0mb** → **IM0mb**. These intermediates after the proton transfer, **IM0ma** and **IM0mb**, are the precursors for the ensuing C−C bond cleavage and have two important characteristics. First, a weak interaction between Rh and O(1)H₂ can lead to the dissociation of a water molecule to generate a vacant site. Second, a strong and short Rh−O3 bond decreases the distance between Rh and the substrate, compared with the reactant complexes **RCma** and **RCmb**, and promotes interaction between them.

3.3. C−C Bond Cleavage: C_{sp^3}−C_{sp^3} vs C_{sp^3}−C_{sp^2} and Site Selectivity. Starting from the proton-transferred intermediates **IM0ma** and **IM0mb**, pathways to cleave C_{sp^3}−C_{sp^3} and C_{sp^3}−C_{sp^2} bonds are studied in detail. The reaction scheme and the energy profiles are also shown in Scheme 4 and Figure 2.

3.3.1. Transition States of C−C Bond Cleavage with Water Coordinating to Rh. From **IM0ma** and **IM0mb**, transition-state structures **TS12a_w_iso(sp³)** and **TS12b_w_iso(sp²)** were obtained, corresponding to the cleavage of C_{sp^3}−C_{sp^3} and C_{sp^3}−C_{sp^2} bonds, respectively (path no. 1 in Figure 2). The Rh−O1 distances (2.218 and 2.241 Å) at these TSs indicate that the newly formed water stays in the complex coordinating to Rh (Figure 4). The barriers for both TSs are too high for this reaction pathway to be important.
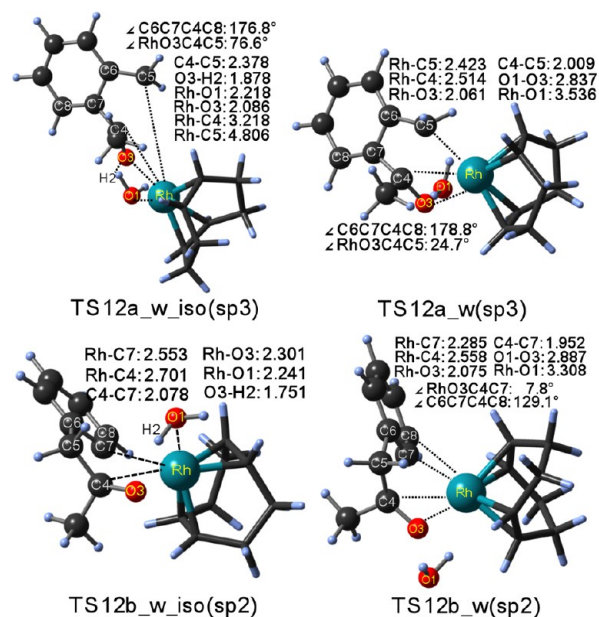

Figure 4. Selected geometrical parameters (in Å and °) of four transition states **TS12a_w_iso(sp³)**, **TS12b_w_iso(sp²)**, **TS12a_w-(sp³)**, and **TS12b_w(sp²)** for C−C bond cleavage with H₂O coordinated.

3.3.2. Transition States of C−C Bond Cleavage with Water Coordinating to O3. Considering the possibility that the newly formed water forms H-bonding with O3 during the C−C cleavage process, two transition-state structures, **TS12b_w(sp²)** and **TS12a_w(sp³)**, respectively, are obtained (path no. 2 in Figure 2). The O1−O3 distances 2.887 Å in **TS12b_w(sp²)** and 2.887 Å in **TS12a_w(sp³)** indicate the formation of H-bonding, while the increasing Rh−O1 distances of 3.308 Å in **TS12b_w(sp²)** and 3.536 Å in **TS12a_w(sp³)** indicate the dissociation of water from Rh (Figure 4). The water molecule comes away from the first coordination shell into the second solvation shell. The other Rh-coordinate distances in **TS12b_w(sp²)** and in **TS12a_w(sp³)** are shorter than those corresponding bonds in **TS12b_w_iso(sp²)** and **TS12a_w_iso(sp³)**, showing that the coordination becomes stronger when the number of ligands coordinating to Rh is reduced. The energy barrier for **TS12b_w(sp²)** is 12.6 kcal/mol and that for **TS12a_w(sp³)** is 14.2 kcal/mol, much lower than the corresponding energy barrier at **TS12b_w_iso(sp²)** and **TS12a_w_iso(sp³)**. This suggests that the stronger

coordination lowers the barriers efficiently. These pathways are a little higher in free energy than the pathways with water fully removed, as will be discussed in the next subsection.

3.3.3. Transition States of C−C Bond Cleavage after Water Removal. An examination of TS structures in the preceding paragraphs suggests that the water molecule may be taking up a coordination site on Rh, resulting in an increase of the barrier for C−C cleavage. The high reaction temperature (100 °C) required may entropically favor water dissociation. Two intermediates (**IM1a** and **IM1b**) were found (Figure 5)
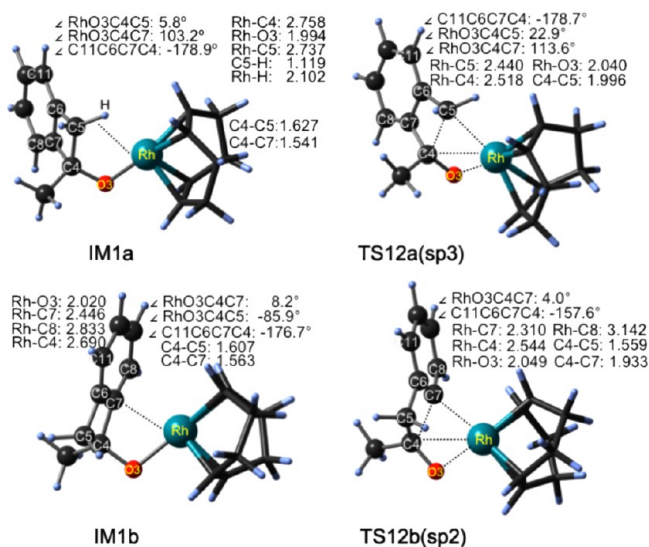

Figure 5. Selected geometrical parameters (in Å and °) of two intermediates after water removal, **IM1a** and **IM1b**, and C−C bond cleavage transition state **TS12a(sp³)** and **TS12b(sp²)**.

after the removal of water from **IM0ma** and **IM0mb**, respectively. In **IM1b**, the generated vacant site interacts strongly with the C7−C8 π-bond to form the η¹- or distorted η²-benzene complex.[17] The coordination elongates the C4−C7 bond by 0.02 Å from **IM0mb**. On the other hand, an agostic interaction is present in the structure of **IM1a**, which might be characterized as involving an η³-C4−C5−H interaction; both C4−C5 and C5−H bonds are elongated by 0.02 Å, respectively.

This water dissociation step is slightly (2.6−7.5 kcal/mol) endothermic in free energy (path no. 3 of Figure 2). Very interestingly, **IM1b** is 4.9 kcal/mol lower than **IM1a**. The EDA of these structures in Table 2 indicates that this energy

Table 2. EDA for the Gibbs Energy Difference (ΔG) between Two Intermediates (IM1a and IM1b) and Two Transition States (TS12a(sp³) and TS12b(sp²)) with cod in Toluene at B3LYP/BS2 Level

	ΔG	ΔDEF (Cat, Sub)	ΔINT
IM1a, IM1b	4.93	−0.13 (−0.05, −0.09)	5.07
TS12a(sp³), TS12b(sp²)	2.46	−4.22 (−0.17, −4.06)	6.68

difference between **IM1b** and **IM1a** is mainly derived from the difference in the interaction energy, and the deformation energy has little effect. The interaction of the rhodium with the benzene ring in **IM1b** is more stabilizing than the agostic interaction in **IM1a**.

Starting from the intermediates **IM1a** and **IM1b**, transition-state structures **TS12a(sp³)** and **TS12b(sp²)** were located,

respectively (Figure 6). These barriers without participation of water is lower than those with coordinating water by 2.7 and 1.8 kcal/mol for C_{sp^3}−C_{sp^2} and C_{sp^3}−C_{sp^3} bond cleavage, respectively (path no. 4 of Figure 2). Relative to the starting point **RCma**, the free energy of **TS12b(sp²)** is 9.9 kcal/mol, which is lower by 2.5 kcal/mol than that of **TS12a(sp³)** (12.4 kcal/mol). Thus the barrier for C_{sp^3}−C_{sp^2} bond activation is lower than that for C_{sp^3}−C_{sp^3} bond activation. Now, a total reversal of the activation of C_{sp^3}−C_{sp^2} vs C_{sp^3}−C_{sp^3} bond cleavage is verified (see Figure S3); under thermal conditions, the C_{sp^3}−C_{sp^2} barrier was about 27 kcal/mol higher than the C_{sp^3}−C_{sp^3} barrier.

One notices that the preference of transition state **TS12b(sp²)** relative to **TS12a(sp³)**, 2.5 kcal/mol, is smaller than that of reactant complex **IM1b** relative to **IM1a**, 4.9 kcal/mol. As discussed already, the EDA in Table 2 for the free energy difference showed that **IM1b** is more stable than **IM1a** because the interaction energy ΔINT is more favorable (5.1 kcal/mol) for **IM1b** due to strong η¹ catalyst−substrate interaction. EDA also shows that ΔINT is even more favorable to **TS12b(sp²)** as much as 6.7 kcal/mol. However, there is a large opposite contribution of ΔDEF, −4.2 kcal/mol, essentially all coming from the distortion of the substrate, which reduces the preference of **TS12b(sp²)** relative to **TS12a(sp³)** in ΔG to 2.5 kcal/mol. This shows that **TS12b(sp²)** has to distort the geometry more seriously from the reactant complex **IM1b** than **TS12a(sp³)** has to do from **IM1a**. This is quite reasonable as the ∠C11−C6−C7−C4 dihedral angle has to change from almost planar −176.7° in **IM1b** to −157.6° in **TS12b(sp²)**, while the corresponding change from −178.9° in **IM1a** to −178.7° in **TS12a(sp³)** is smaller (see Figure 5). A very important fact is, despite this additional deformation energy requirement, Csp^3−Csp^2 bond activation is easier than Csp^3−Csp^3 bond activation. The advantage gained by the interaction of the metal center with the C7−C8 π-bond in **IM1b** is still retained in the critical TS of **TS12b(sp²)**.

3.3.4. Solvent Effect on the Transition States of C−C Bond Cleavage. The influence of the DMSO as the solvent was also theoretically considered using PCM model (DMSO, ε = 46.826). The calculated energy difference 1.9 kcal/mol between **TS12a(sp³)** and **TS12b(sp²)** in DMSO is smaller than the difference 2.5 kcal/mol in toluene (see Table S3), indicating that the site selectivity should become worse. This is consistent with the experimental results in DMSO that DP (product of the C_{sp^3}−C_{sp^2} ("proximal") bond cleavage) yield was 63% along with TP (product of the C_{sp^3}−C_{sp^3} ("distal") bond cleavage) yield of 31% yield (Table 1). The reduced energy difference is due to the different sensitivity of the structures to the polar environment. When the solvent environment changes from toluene to DMSO, the energy of **TS12a(sp³)** is lowered by 3.5 kcal/mol, which is a little more than that of **TS12b(sp²)** (2.9 kcal/mol), reducing the preference of **TS12b(sp²)**. The larger stabilization of **TS12a(sp³)** by DMSO can be ascribed to its larger polarity. The dipole moment of **TS12a(sp³)** is 3.34 D, which is a little larger than that of **TS12b(sp²)** (2.47 D). The Mulliken charge analysis in DMSO shows that the electron density at O3 of **IM1a** (−0.601) is decreased to be −0.503 at O3 of **TS12a(sp³)**, while the electron density on C4 (0.310) and C5 (−0.460) is increased to be 0.266 and −0.553, respectively, which indicates that there is a charge transfer from O3 to C4−C5 bond during the ring-opening process. Similar phenomena could be observed from **IM1b** to **TS12b(sp²)**.
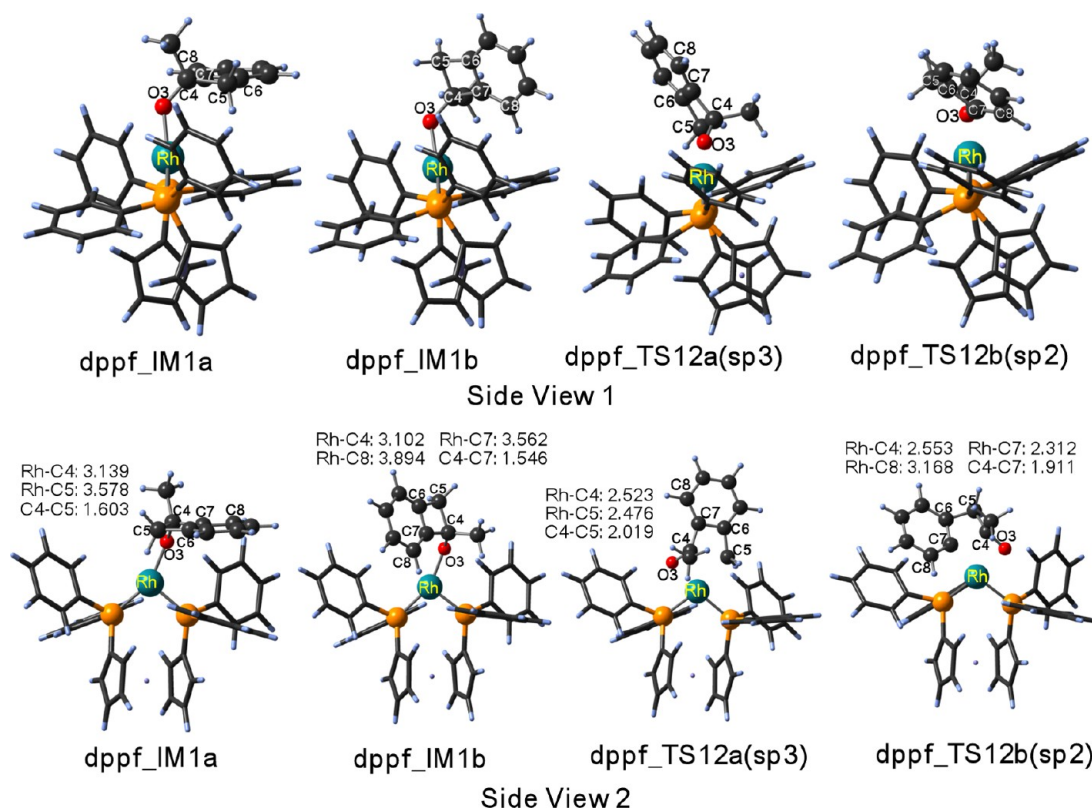
Figure 6. Selected geometrical parameters (in Å) of the intermediates and transition state for the reaction with the DPPF ligand.

3.3.5. Two Intermediates IM2a and IM2b. Once the C—C bond cleavage takes place, there is a sharp energy decrease (30—40 kcal/mol) due to the relief of the structural strain. The highly strained four-membered ring in **TS12a(sp^3)** and **TS12b(sp^2)** is opened, and the six-membered rings are formed in **IM2a** and **IM2b**. Different from the first intermediates (**IM1a** and **IM1b**), which would be in thermal equilibrium, the ratio of the second intermediates (**IM2a** and **IM2b**), i.e., the site selectivity of the C—C cleavage products, should be kinetically determined by the barriers at **TS12a(sp^3)** and **TS12b(sp^2)**.

3.4. Final Proton Transfer for Product Formation and Active Species Recovery. To produce the final product and regenerate the active species, one water is needed to provide proton to the product and OH to the rhodium (Scheme 4). Initially, the water complexes (**IM2a_w** and **IM2b_w**) are formed when one water molecule coordinates to **IM2a** and **IM2b**, respectively. The endothermicity of water coordination (5—7 kcal/mol) is due to the entropic contribution. Starting from the intermediates **IM2a_w** and **IM2b_w**, four-membered ring transition states, referred as **TS23a** and **TS23b**, are obtained, respectively, which lead to the formation of the final product complex (**IM3a(AC·TP)** and **IM3b(AC·DP)**). Since **IM2a** and **IM2b** are in deep minima and the final proton transfer requires activation energies, this process should be accelerated by heating but should not affect the overall rate constant of the entire reaction. This is consistent with the experiment that the ring-opening reaction in Scheme 1 requires heating, while alkyne insertion reaction proceeds even at room temperature (Scheme 5). The replacement of the product ligand in **IM3**'s by a reactant ligand will regenerate the starting active species **RC**'s in the catalytic cycle; we did not study this step.

Scheme 5. Alkyne Insertion into Benzocyclobutenol
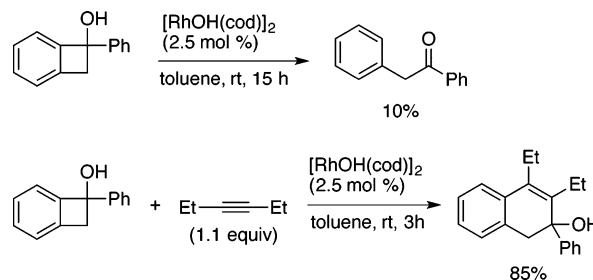
3.5. Effects of Ligands on the Site Selectivity. Experimentally, the site selectivity is dependent upon the ligands of the rhodium complex (Table 1). When the cod ligand was replaced with DPPF, DP was obtained in 35% yield together with TP in 50% yield. The use of P(t-Bu)$_3$ as the ligand afforded DP in 74% yield and TP in 14% yield. In order to gain insight into the effect of ligands, we computationally investigated the key steps by employing DPPF and P(t-Bu)$_3$ in place of cod in the toluene PCM solvent.

3.5.1. Site Selectivity with Ligand DPPF. Using DPPF as the ligand, two proton-transferred dehydrated intermediates, **dppf_IM1a** and **dppf_IM1b**, have been obtained within toluene following the pathways discussed in Section 3.4. As shown in Figure 6, the quite similar and long distances Rh—C5 (3.577 Å) for **dppf_IM1a** and Rh—C7 (3.562 Å) for **dppf_IM1b** show that there is no preference for either C$_{sp^2}$ or C$_{sp^3}$ side, the situation different from that with cod. No strong interaction of Rh with C7—C8 π-bond can be seen in **dppf_IM1b**. The free energy of **dppf_IM1b** is only 1.20 kcal/mol lower than **dppf_IM1a**, which is much smaller than ~6 kcal/mol between **IM1b** and **IM1a** with cod. The differences
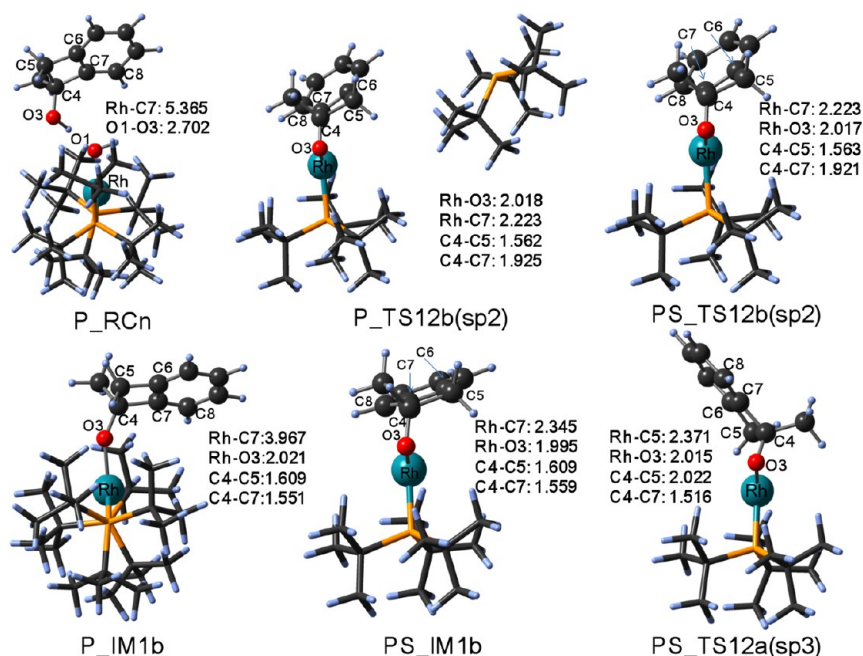
Figure 7. Selected geometrical parameters (in Å) of the key intermediates and transition states for the P(t-Bu)$_3$ ligands, at B3LYP/BS1 level in gas phase.

between **dppf_IM1b** and **dppf_IM1a** in DEF (0.75 kcal/mol) and INT (0.46) are very small (Table S3). The clear decrease of the contribution of INT in the stabilization of **IM1b**-type intermediate is due to the less back-donating character of the DPPF ligand.

From these two intermediates, two transition-state structures (**dppf_TS12a(sp^3)** and **dppf_TS12b(sp^2)**) are obtained. The relative energy of **dppf_TS12a(sp^3)** is slightly lower (by 0.3 kcal/mol) to **dppf_TS12b(sp^2)**. The loss or reverse of site selectivity is in good agreement with the experimental observation. EDA in Table S2 shows that **dppf_TS12b(sp^2)** has stronger interaction (about 10 kcal/mol more favorable INT) than **dppf_TS12a(sp^3)**, but the price to pay for deformation of both substrate and metal complex more than upsets the advantage of INT.

The structure overlap between **dppf_IM1b** and **dppf_TS12b(sp^2)** (Figure S6) shows that a dihedral angle significantly deforms (∠C11−C6−C7−C4: from −178.6° for **dppf_IM1b** to −148.3° for **dppf_TS12b(sp^2)**) in the substrate part, while in the catalyst part the dppf ligand rotates and dissociates a little bit (Rh−P: 2.217−2.249 to 2.272−2.309 Å) to reach a proper position.

The calculations including dispersion at B3LYP-D3/BS2//B3LYP/BS1 and B3LYP-D3/BS2//B3LYP-D3/BS2 level, as shown in Table S4, however, predict that the dispersion makes **TS12b(sp^2)** to be more stable than **TS12a(sp^3)** by 3.7 kcal/mol, in contradiction with the experiment of loss of selectivity as well as the value of −0.3 kcal/mol without dispersion at B3LYP/BS2//B3LYP/BS1 level discussed above. The detailed EDA analysis in Tables S3 and S4 indicates that the dispersion stabilizes **TS12b(sp^2)** about 3.6 kcal/mol more than **TS12a-(sp^3)** changing the balance. We suspect that B3LYP-D3 calculations are overestimating the dispersion contribution, in particular, between Fe and the carbon π orbital, but will be reexamined in detail in the future.

B. Site Selectivity with Ligand P(t-Bu)$_3$. The coordination of Rh with two P(t-Bu)$_3$ ligands is more crowded than that with

the DPPF ligand. Surprisingly for this system DP (C$_{sp^3}$−C$_{sp^2}$ bond cleavage product) is experimentally preferred over TP (C$_{sp^3}$−C$_{sp^3}$ bond cleavage product), which is the same site selectivity with cod but different from DPPF. Theoretical consideration could provide a reasonable insight into this ligand effect. The optimized reactant complexes with two P(t-Bu)$_3$ ligands have long intermolecular distances, Rh−C5 = 5.410 Å and O1−O3 = 2.699 Å in **P_RCm** and Rh−C7 = 5.365 Å and O1−O3 = 2.702 Å in **P_RCn** (Figures 7 and S5), indicating that the coordination interaction and H-bond between the substrate and rhodium complex are much weaker than those with cod ligand. The optimization trials to obtain proton-transfer transition-state structure failed to provide such structures, and we conclude that such pathways do not exist or have quite high energies. It seems that the activation region is too crowded.

Thus, the intermediate **P_IM1b** (Figure 7) after the removal of water was taken as the starting point. The distance of Rh−C$_{sp^2}$ (3.967 Å) in **P_IM1b** shows that the interaction is quite weak. No transition state for C−C bond cleavage, like **TS12b(sp^2)** for cod, could be located by standard TS search. From **P_IM1b** a relaxed scan for Rh−C7 followed by TS optimization (Figure S6) resulted in a TS structure **P_TS12b-(sp^2)** (Figure 7); in this structure one P(t-Bu)$_3$ ligand has spontaneously moved out of the Rh site. The situation is similar for the sp^3 side of approach.

It is concluded that one of the phosphines has to dissociate during the reaction, and the active catalyst is RhP(t-Bu)$_3$ with coordinate unstaturation. Starting from RhP(t-Bu)$_3$, the reaction pathways have been followed in the same way as for the cod ligand. As shown in Figure S7, the reaction proceeds smoothly from the reactant−catalyst complexes **PS_RCm** and **PS_RCm**, to the proton-transfer intermediates, **PS_IM0m** and **PS_IM0n**, followed by water dissociation to give strongly interacting intermediates **PS_IM1a** and **PS_IM1b** (Figure 7). **PS_IM1b** goes over **PS_TS12b(sp^2)**, the TS for C$_{sp^3}$−C$_{sp^2}$ bond cleavage, to reach very exothermically the open-ring

intermediate **PS_IM2b**, before coordinating on water molecule to give **PS_IM2b_w** for the final proton transfer to generate the product and active catalyst. On the other hand, **PS_IM1a** → **PS_TS12a(sp^3)** (Figure 7) → **PS_IM2** → **PS_IM2a_w** provides the $C_{sp^3}-C_{sp^3}$ cleavage product. It should be noted that the Gibbs free energy of the $C_{sp^3}-C_{sp^2}$ TS **PS_TS12b(sp^2)** is 4.2 kcal/mol lower than that of the $C_{sp^3}-C_{sp^3}$ TS **PS_TS12a-(sp^3)** at B3LYP/BS2 level which should be even larger with considering the dispersion correction. That is to say that the $C_{sp^3}-C_{sp^2}$ site selectivity is obtained, in good agreement with the experiment. This is because strong interaction between the catalyst and the substrate at the C−C cleavage TS is recovered in the mono-phosphine active catalyst as in the cod catalyst.

4. CONCLUSIONS

We have systematically investigated the site-selective reaction mechanism of Rh-catalyzed ring opening of benzocyclobutenol with the model catalyst $[Rh(OH)(cod)]_2$ and the factors controlling its site selectivity such as solvent environment and ligands (DPPF and $P(t\text{-Bu})_3$) by the DFT. The Rh-catalyzed ring-opening reaction proceeds in three steps. First proton transfer from the substrate to the active Rh catalyst to form the precursor for the next step. Weak interaction between Rh and OH_2 leads to the dissociation of a water molecule to generate a vacant site. The water-dissociated intermediate shows short Rh−O3 bond distance and simultaneously increases in the interaction between Rh and the substrate. The next C−C cleavage step giving the ring-opened intermediates determines the site selectivity. Against the thermodynamics of the $C_{sp^3}-C_{sp^2}$ and $C_{sp^3}-C_{sp^3}$ bond strengths, the $C_{sp^3}-C_{sp^2}$ cleavage is favored over the $C_{sp^3}-C_{sp^3}$ cleavage in this catalysis because the former transition state is stabilized by an interaction between the benzene ring of the substrate and the Rh, while in the latter such interaction does not exist. Finally, a water molecule coordinates back to the opened intermediates, followed by proton transfer from water to the product substrate that is eventually released to give the final product and regenerates the active catalyst.

The polar solvent, DMSO, compared with toluene, reduces the site selectivity in the C−C cleavage step. The polar DMSO lowers the energy of TS for $C_{sp^3}-C_{sp^3}$ cleavage more than that of $C_{sp^3}-C_{sp^2}$ cleavage, because the former is more polar with larger dipole moment, and the advantage of **TS12b(sp^2)** over **TS12a(sp^3)** is reduced. This reduction of site selectivity in polar solvent is consistent with the experimental finding.

Steric effects from the ligand play an important role in the different site selectivity between cod and DPPF. Calculations show that the advantage of the TS for $C_{sp^3}-C_{sp^2}$ cleavage over that of $C_{sp^3}-C_{sp^3}$ cleavage is reduced to a minimum with DPPF. Energy decomposition analysis shows that the TS for $C_{sp^3}-C_{sp^2}$ cleavage still has stronger interaction energy (about 10 kcal/mol) between the substrate and the catalyst compared to that for $C_{sp^3}-C_{sp^3}$ cleavage but that the price to pay for deformation both for substrate and catalyst for the tight $C_{sp^3}-C_{sp^2}$ TS in this sterically crowded DPPF system nearly totally upsets the advantage of the interaction energy.

Then why in the experiment can the even more crowded $Rh(P(t\text{-Bu})_3)_2$ produce a better site selectivity than that DPPF does? Calculations show that $Rh(P(t\text{-Bu})_3)_2$ is overcrowded, and one of the two phosphines has to dissociate for the reaction to take place. With $P(t\text{-Bu})_3$ as the active catalyst that is not overcrowded, the advantage of tight $C_{sp^3}-C_{sp^2}$ TS is recovered

(compared with DPPF), and a reasonable selectivity of $C_{sp^3}-C_{sp^2}$ cleavage is predicted, again consistent with the experiment.

The insight provided by the present theoretical calculations and analysis should provide important guiding principles for designing better catalysts for the site selectivity.

■ ASSOCIATED CONTENT

Ⓢ Supporting Information

Complete ref 9, Scheme S1, Figures S1−S7, Tables S1−S3, and Cartesian coordinates of the optimized structures. This material is available free of charge via the Internet at http://pubs.acs.org.

■ AUTHOR INFORMATION

Corresponding Author

morokuma@fukui.kyoto-u.ac.jp

Notes

The authors declare no competing financial interest.

■ ACKNOWLEDGMENTS

■ REFERENCES

(1) For general reviews: (a) Crabtree, R. H. *Chem. Rev.* **1985**, *85*, 245−269. (b) Halpern, J. *Inorg. Chim. Acta* **1985**, *100*, 41−48. (c) Shilov, A. E.; Shul'pin, G. B. *Chem. Rev.* **1997**, *97*, 2879−2932. (d) Jones, W. D. *Top. Organomet. Chem.* **1999**, 9−46. (e) Kakiuchi, F.; Murai, S. *Top. Organomet. Chem.* **1999**, 47−79. (f) Jia, C.; Kitamura, T.; Fujiwara, Y. *Acc. Chem. Res.* **2001**, *34*, 633−639. (g) *Handbook of C−H Transformations*; Dyker, G., Ed.; Wiley-VCH: Weinheim, Germany, 2005. (h) Daugulis, O.; Do, H.-Q.; Shabashov, D. *Acc. Chem. Res.* **2009**, *42*, 1074−1086. (i) Giri, R.; Shi, B.-F.; Engle, K. M.; Maugel, N.; Yu, J.-Q. *Chem. Soc. Rev.* **2009**, *38*, 3242−3272. (j) Colby, D. A.; Bergman, R. G.; Ellman, J. A. *Chem. Rev.* **2010**, *110*, 624−655. (k) Mkhalid, I. A. I.; Barnard, J. H.; Marder, T. B.; Murphy, J. M.; Hartwig, J. F. *Chem. Rev.* **2010**, *110*, 890−931. (l) Lyons, T. W.; Sanford, M. S. *Chem. Rev.* **2010**, *110*, 1147−1169. (m) Ackermann, L. *Chem. Commun.* **2010**, *46*, 4866−4877. (n) Newhouse, T.; Baran, P. S. *Angew. Chem., Int. Ed.* **2011**, *50*, 3362−3374. (o) McMurray, L.; O'Hara, F.; Gaunt, M. J. *Chem. Soc. Rev.* **2011**, *40*, 1885−1898. (p) Yeung, C. S.; Dong, V. M. *Chem. Rev.* **2011**, *111*, 1215−1292. (q) Sun, C.-L.; Li, B.-J.; Shi, Z.-J. *Chem. Rev.* **2011**, *111*, 1293−1314. (r) Cho, S. H.; Kim, J. Y.; Kwak, J.; Chang, S. *Chem. Soc. Rev.* **2011**, *40*, 5068−5083. (s) Kuhl, N.; Hopkinson, M. N.; Wencel-Delord, J.; Glorius, F. *Angew. Chem., Int. Ed.* **2012**, *51*, 10236−10254. (t) Yamaguchi, J.; Yamaguchi, A. D.; Itami, K. *Angew. Chem., Int. Ed.* **2012**, *51*, 8960−9009. (u) Arockiam, P. B.; Bruneau, C.; Dixneuf, P. H. *Chem. Rev.* **2012**, *112*, 5879−5918.

(2) For general reviews: (a) Rybtchinski, B.; Milstein, D. *Angew. Chem., Int. Ed.* **1999**, *38*, 870−883. (b) Murakami, M.; Ito, Y. *Top. Organomet. Chem.* **1999**, 97−129. (c) Takahashi, T.; Kotora, M.; Hara, R.; Xi, Z. *Bull. Chem. Soc. Jpn.* **1999**, *72*, 2591−2602. (d) Perthuisot, C.; Edelbach, B. L.; Zubris, D. L.; Simhai, N.; Iverson, C. N.; Müller,

C.; Satoh, T.; Jones, W. D. *J. Mol. Cat. A* **2002**, *189*, 157−168. (e) Jun, C.-H. *Chem. Soc. Rev.* **2004**, *33*, 610−618. (f) Miura, M.; Satoh, T. *Top. Organomet. Chem.* **2005**, *14*, 1−20. (g) Kondo, T.; Mitsudo, T. *Chem. Lett.* **2005**, *34*, 1462−1466. (h) Nečas, D.; Kotora, M. *Curr. Org. Chem.* **2007**, *11*, 1566−1591. (i) Tobisu, M.; Chatani, N. *Chem. Soc. Rev.* **2008**, *37*, 300−307. (j) Nakao, Y.; Hiyama, T. *Pure Appl. Chem.* **2008**, *80*, 1097−1107. (k) Yorimitsu, H.; Oshima, K. *Bull. Chem. Soc. Jpn.* **2009**, *82*, 778−792. (l) Seiser, T.; Cramer, N. *Org. Biomol. Chem.* **2009**, *7*, 2835−2840. (m) Bonesi, S. M.; Fagnoni, M. *Chem.—Eur. J.* **2010**, *16*, 13572−13589. (n) Murakami, M.; Matsuda, T. *Chem. Commun.* **2011**, *47*, 1100−1105. (o) Aïssa, C. *Synthesis* **2011**, 3389−3407. (p) Ruhland, K. *Eur. J. Org. Chem.* **2012**, 2683−2706.

(3) (a) Nishimura, T.; Ohe, K.; Uemura, S. *J. Am. Chem. Soc.* **1999**, *121*, 2645−2646. (b) Matsuda, T.; Makino, M.; Murakami, M. *Org. Lett.* **2004**, *6*, 1257−1259. (c) Matsuda, T.; Makino, M.; Murakami, M. *Bull. Chem. Soc. Jpn.* **2005**, *78*, 1528−1533. (d) Seiser, T.; Cramer, N. *J. Am. Chem. Soc.* **2010**, *132*, 5340−5341.

(4) (a) Nishimura, T.; Uemura, S. *Synthesis* **2004**, 201−216. (b) Murakami, M. *Chem. Rec.* **2010**, *10*, 326−331. (c) Cramer, N.; Seiser, T. *Synthesis* **2010**, 449−460.

(5) (a) Ishida, N.; Sawano, S.; Masuda, Y.; Murakami, M. *J. Am. Chem. Soc.* **2012**, *134*, 17502−17504. For related ring-opening reactions of benzocyclobutenols and cyclobutenols, see: (b) Chtchemelinine, A.; Rosa, D.; Orellana, A. *J. Org. Chem.* **2011**, *76*, 9157−9162. (c) Matsuda, T.; Miura, N. *Org. Biomol. Chem.* **2013**, *11*, 3424−3427. (d) Rosa, D.; Chtchemelinine, A.; Orellana, A. *Synthesis* **2012**, *76*, 1885−1891.

(6) (a) Evans, M. E.; Li, T.; Jones, W. D. *J. Am. Chem. Soc.* **2010**, *132*, 16278−16284. (b) Atesin, T. A.; Li, T.; Lachaize, S.; Garca, J. J.; Jones, W. D. *Organometallics* **2008**, *27*, 3811−3817. (c) Li, T.; Garcia, J. J.; Brennessel, W. W.; Jones, W. D. *Organometallics* **2010**, *29*, 2430−2445. (d) Jiang, Y.-Y.; Yu, H.-Z.; Fu, Y. *Organometallics* **2013**, *43*, 926−936. (e) Obenhuber, A.; Ruhland, K. *Organometallics* **2011**, *30*, 4039−4051. (f) Montag, M.; Efremenko, I.; Diskin-Posner, Y.; Ben-David, Y.; Martin, J. M. L.; Milstein, D. *Organometallics* **2012**, *31*, 505−512. (g) Rybtchinski, B.; Oevers, S.; Montag, M.; Vigalok, A.; Rozenberg, H.; Martin, J. M. L.; Milstein, D. *J. Am. Chem. Soc.* **2001**, *123*, 9064−9077. (h) Khoroshun, D. V.; Inagaki, A.; Suzuki, H.; Vyboishchikov, S. F.; Musaev, D. G.; Morokuma, K. *J. Am. Chem. Soc.* **2003**, *125*, 9910−9911. (i) Chaplin, A. B.; Tonner, R.; Weller, A. S. *Organometallics* **2010**, *29*, 2710−2714. (j) Darmon, J. M.; Stieber, S. C. E.; Sylvester, K. T.; Fernandez, I.; Lobkovsky, E.; Semproni, S. P.; Bill, E.; Wieghardt, K.; DeBeer, S.; Chirik, P. J. *J. Am. Chem. Soc.* **2012**, *134*, 17125−17137. (k) Sakaki, S.; Ohki, T.; Takayama, T.; Sugimoto, M.; Kondo, T.; Mitsudo, T. *Organometallics* **2001**, *20*, 3145−3158. (l) Zhang, S.-L.; Fu, Y.; Shang, R.; Guo, Q.-X.; Liu, L. *J. Am. Chem. Soc.* **2010**, *132*, 638−646. (m) Xue, L.; Su, W.; Lin, Z. *Dalton Trans.* **2010**, *39*, 9815−9822. (n) García-Fandiño, R.; Gulías, M.; Castedo, L.; Granja, J. R.; Mascareñas, J. L.; Cárdenas, D. J. *Chem.—Eur. J.* **2008**, *14*, 272−281. (o) An, Y.; Cheng, C.; Pan, B.; Wang, Z. *Eur. J. Org. Chem.* **2012**, 3911−3915.

(7) (a) Parr, R. G.; Yang, W. *Density functional Theory of Atoms and Molecules*; Oxford University Press: Oxford, 1989. (b) Cramer, C. J.; Truhlar, D. G. *Phys. Chem. Chem. Phys.* **2009**, *11*, 19757−10816.

(8) (a) Scalmani, G.; Frisch, M. J. *J. Chem. Phys.* **2010**, *132*, 114110. (b) Tomasi, J.; Mennucci, B.; Cammi, R. *Chem. Rev.* **2005**, *105*, 2999−3093.

(9) Frisch, M. J.; et al. *Gaussian 09*, revision A.1; Gaussian, Inc., Wallingford, CT, 2009.

(10) Becke, A. D. *Phys. Rev. A* **1988**, *38*, 3098−3100.

(11) (a) Lee, C.; Yang, W.; Parr, R. G. *Phys. Rev. B* **1988**, *37*, 785−89. (b) Miehlich, B.; Savin, A.; Stoll, H.; Preuss, H. *Chem. Phys. Lett.* **1989**, *157*, 200−06.

(12) (a) Petersson, G. A.; Bennett, A.; Tensfeldt, T. G.; Al-Laham, M. A.; Shirley, W. A.; Mantzaris, J. *J. Chem. Phys.* **1988**, *89*, 2193−218. (b) Petersson, G. A.; Al-Laham, M. A. *J. Chem. Phys.* **1991**, *94*, 6081−90.

(13) Zhao, Y.; Truhlar, D. G. *Theor. Chem. Acc.* **2008**, *120*, 215−41.

(14) (a) Fukui, K. *Acc. Chem. Rec.* **1981**, *14*, 363−368. (b) Fukui, K. *J. Phys. Chem.* **1970**, *74*, 4161−4163.

(15) (a) Hermans, J.; Wang, L. *J. Am. Chem. Soc.* **1997**, *119*, 2707−2714. (b) Yu, Z.-X.; Houk, K. N. *J. Am. Chem. Soc.* **2003**, *125*, 13825−13830. (c) Sugiyama, A.; Ohnishi, Y.-y.; Nakaoka, M.; Nakao, Y.; Sato, H.; Sakaki, S.; Nakao, Y.; Hiyama, T. *J. Am. Chem. Soc.* **2008**, *130*, 12975−12985. (d) Tanaka, R.; Yamashita, M.; Chung, L. W.; Morokuma, K.; Nozaki, K. *Organometallics* **2011**, *30*, 6742−6750.

(16) (a) Kina, A.; Iwamura, H.; Hayashi, T. *J. Am. Chem. Soc.* **2006**, *128*, 3904−3905. (b) Kina, A.; Yasuhara, Y.; Nishimura, T.; Iwamura, H.; Hayashi, T. *Chem. Asian J.* **2006**, *1*, 707−711.

(17) (a) Zhao, P.; Incarvito, C. D.; Hartwig, J. F. *J. Am. Chem. Soc.* **2006**, *128*, 3124−3125. (b) Zhao, P.; Hartwig, J. F. *Organometallics* **2008**, *27*, 4749−4757.

178

dx.doi.org/10.1021/ja407422q | *J. Am. Chem. Soc.* 2014, 136, 169−178